

Influence of different open circuit voltage tests on state of charge online estimation for lithium-ion batteries

Fangdan Zheng ^{a,b}, Yinjiao Xing ^b, Jiuchun Jiang ^{a,*}, Bingxiang Sun ^a, Jonghoon Kim ^c, Michael Pecht ^b

^a National Active Distribution Network Technology Research Center (NANTEC), Collaborative Innovation Center of Electric Vehicles in Beijing, Beijing Jiaotong University, Beijing 100044, China

^b Center for Advanced Life Cycle Engineering (CALCE), University of Maryland, College Park, MD 20742, USA

^c Energy Storage Conversion Laboratory (ESCL), Chungnam National University, Yuseong-gu, Daejeon 34134, Republic of Korea



HIGHLIGHTS

- Two common tests for observing battery open circuit voltage performance are compared.
- The temperature dependency of the OCV-SOC relationship is investigated.
- Two estimators are evaluated in terms of accuracy and robustness for estimating battery SOC.
- The incremental OCV test is better to predetermine the OCV-SOCs for SOC online estimation.

ARTICLE INFO

Article history:

Received 15 July 2016

Received in revised form 2 September 2016

Accepted 3 September 2016

Available online 10 September 2016

Keywords:

Lithium-ion batteries

Battery management system

State of charge estimation

Open circuit voltage

Temperature dependency

ABSTRACT

Battery state of charge (SOC) estimation is a crucial function of battery management systems (BMSs), since accurate estimated SOC is critical to ensure the safety and reliability of electric vehicles. A widely used technique for SOC estimation is based on online inference of battery open circuit voltage (OCV). Low-current OCV and incremental OCV tests are two common methods to observe the OCV-SOC relationship, which is an important element of the SOC estimation technique. In this paper, two OCV tests are run at three different temperatures and based on which, two SOC estimators are compared and evaluated in terms of tracking accuracy, convergence time, and robustness for online estimating battery SOC. The temperature dependency of the OCV-SOC relationship is investigated and its influence on SOC estimation results is discussed. In addition, four dynamic tests are presented, one for estimator parameter identification and the other three for estimator performance evaluation. The comparison results show that estimator 2 (based on the incremental OCV test) has higher tracking accuracy and is more robust against varied loading conditions and different initial values of SOC than estimator 1 (based on the low-current OCV test) with regard to ambient temperature. Therefore, the incremental OCV test is recommended for predetermining the OCV-SOCs for battery SOC online estimation in BMSs.

© 2016 Elsevier Ltd. All rights reserved.

1. Introduction

The rapid development of electric vehicles (EVs) in the last decade has drawn increasing attention from both industry and academia due to the global energy crisis and demands to reduce greenhouse gases. Different types of batteries, such as lithium, nickel-cadmium, lead-acid, and alkaline, are widely used as the dominant energy source in EVs. In particular, lithium-ion batteries are the most promising and competitive candidates because of their unique features, including their high energy density, long

cycle life, high efficiency, and environmental-friendly performance [1–5]. As a critical component inside an EV, a lithium-ion battery should operate stably to guarantee the safety and reliability of the entire electric system. Therefore, a battery management system (BMS) that performs as a connector between the vehicle and the battery is developed to indicate the state of batteries and avoid abuse of batteries. One of the main concerns of BMSs is battery state of charge (SOC) estimation. SOC is a measure of the amount of charge stored in a battery at the present moment and acts as the equivalent of a “fuel gauge” in an electric vehicle. SOC shows how long the battery will sustain before it is recharged. Accurate SOC estimation can relieve users’ anxiety about running out of battery power. Moreover, it can ensure that batteries operate

* Corresponding author.

E-mail address: jcjiang@bjtu.edu.cn (J. Jiang).

appropriately within desired limits and thus can prolong a battery's useful life by avoiding over-charging or over-discharging. However, battery SOC cannot be measured directly but must be inferred from observed variables, such as current and voltage. Indeed, many factors can affect the accuracy of SOC estimation results and should be investigated [6]. Therefore, SOC estimation is not only a vital function but also a crucial task of BMS to ensure the safety, efficiency, and longevity of a battery for vehicle life extension.

The following SOC estimation techniques are widely used: the coulomb counting method via the integration of the loading current [7–9]; the data-driven method, which considers a battery as a "black box" and uses machine learning techniques to analyze data [10–12]; and the physical model-based method via equivalent circuit models (ECMs) and electrochemical models [13–21]. In addition, a combination of the above-mentioned methods is used [22–26]. For algorithm implementation in a BMS, a model-based filtering approach is most popular due to its merits: high accuracy, closed-loop, self-corrective ability, and good adaptability. Among battery models, equivalent circuit models (ECMs) are much more practical than electrochemical models since ECMs facilitate estimation schemes with electrical parameters (e.g., charge/discharge current and battery terminal voltage), which are much easier to measure online than electrochemical model parameters (e.g., film resistance and diffusion coefficients). Open circuit voltage (OCV) is a vital element in ECMs because it builds a connection between measured electric parameters and SOC via an OCV-SOC mapping curve. For a certain battery type, its OCV performs as a function of its SOC in nature. The premise of using OCV-SOC is that a battery needs to rest a long time to ensure that its terminal voltage approaches the OCV [6]. However, a long rest time is not practical for EV batteries in the field. Thus filtering techniques based on state-space models are utilized to enhance SOC estimation through combining OCV and coulomb counting [27].

Table 1 shows a common processing method of SOC online estimation for a BMS is shown in **Table 1**. Firstly, the relationship between OCV and SOC is predetermined by an offline OCV-SOC test. The corresponding mapping data is then stored in a BMS as a lookup table or a mathematical function. Secondly, a battery ECM is selected to model the battery dynamic behavior with parameter identification. Lastly, filtering approaches are implemented to enhance model-based SOC online estimation [28]. Efforts have been made to improve the SOC estimation accuracy and the efficiency of a BMS from different aspects. For example, OCV-SOC functions instead of a lookup table have been proposed to describe the relationship between SOC and OCV and thus to save the memory space in a BMS [29–34]. Studies have been conducted on the model selection to pursue a model that can provide high estimation accuracy and also ensure the computational efficiency of a BMS. A first-order resistance-capacitor (RC) model using a parallel RC network to describe the dynamic relaxation effects of the battery is recommended as a model that balances SOC estimation accuracy with model complexity [35]. In addition, different filtering algorithms have been used for online estimation. For instance, the studies in Refs. [6,26,33,36–38] adopted extended Kalman filter, robust extended Kalman filter, and unscented Kalman filter to estimate the SOC. Instead of the Kalman family, the studies in Refs. [39–42] used particle filter, unscented particle filter and dual particle filter to do SOC estimation. Luenberger observer [43] and support vector machine method [44] were also utilized for battery SOC estimation. The performance of different filtering algorithms is compared in terms of tracking accuracy, convergence behavior, and computation time [28].

Several existing issues are seldom addressed in the literature. Firstly, as the basis for SOC online estimation, OCV-SOC tests have not been comprehensively evaluated yet. There are two OCV tests

Table 1
Common processing of SOC online estimation for BMS.

Step 1	OCV-SOC mapping 1. OCV-SOC test 2. Determine OCV-SOC relationship a. OCV-SOC lookup table b. OCV-SOC functions
Step 2	Battery modeling 1. Select a battery equivalent circuit model 2. Model parameter identification
Step 3	Algorithm implementation a. Kalman filter family b. Particle filter

for OCV-SOC mapping commonly used in both industry and academia: the low-current OCV test and the incremental OCV test. One OCV-SOC mapping result differs from another and thus has a different influence on SOC online estimation. It will be helpful to compare two OCV tests and their influence on SOC online estimation results in order to give a suggestion to manufacturers regarding offline predetermined OCV-SOC relationship. Secondly, the temperature dependence of the two OCV-SOC mapping results is rarely investigated. For an existing BMS, an OCV-SOC relationship constructed at a certain temperature (e.g., room temperature) is widely employed [22]. A large error may occur in inferring SOC when the battery is operating at varied temperatures instead of at room temperature, which is typical in the field. Lastly, most SOC online estimation models are validated using a single loading profile and show high estimation accuracy in existing studies [6,23,26,45,46]. But these estimators would perform poorly if they were applied in other working conditions (i.e., using different loading profiles). Therefore, it makes sense to verify the robustness of the SOC estimation approach against varied loading profiles.

This paper innovatively investigates the influence of different OCV tests on online SOC estimation and the temperature dependency of battery OCV characteristic. The main contributions of this paper are as follows: (1) to present a general understanding and a comparison of two OCV-SOC mapping techniques; (2) to investigate the temperature dependency of OCV-SOC curves via two OCV tests, and (3) to show the influence of two OCV tests on SOC online estimation and thus to give a suggestion for predetermining offline the OCV-SOC relationship for practical BMS application.

The remainder of this paper is arranged into five sections. The experiments conducted for this study are introduced in Section 2. Two OCV-SOC mapping results at various temperatures which reflect the temperature dependency of OCV curves is presented in Section 3. Section 4 illustrates the implementation of the SOC online estimation algorithm. Section 5 shows the influence of two OCV tests on the SOC estimation results. A comparison is given using statistics, and the robustness is verified with regard to various experimental cases. Section 6 concludes with a summary of the main findings of this paper.

2. Experiments

As shown in **Fig. 1**, the experimental platform consisted of the test samples, a thermal chamber, an Arbin BT2000 battery test system, and a PC with Arbin software to give test system orders (e.g. charging, discharging) and monitor data information. The test samples were the 18,650 LiNiMnCoO₂/Graphite lithium-ion cells. Their basic specifications are given in **Table 2**. Three separate test schedules were conducted on the battery test bench at low temperature (0 °C), room temperature (25 °C), and high temperature (45 °C), respectively. Test samples were placed inside the chamber so that their ambient temperature was controlled. All the test data were measured and recorded in 1 s intervals.

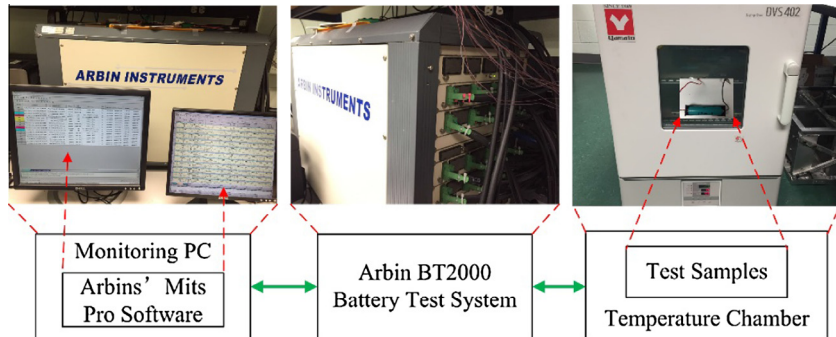


Fig. 1. Battery test platform.

Table 2
Basic specifications of test samples.

Type	Nominal voltage	Nominal capacity	Upper/lower cut-off voltage	Maximum current	Usage temperature
18,650	3.6 V	2.0 Ah	2.5 V/4.2 V	22 A (at 25 °C)	0–50 °C

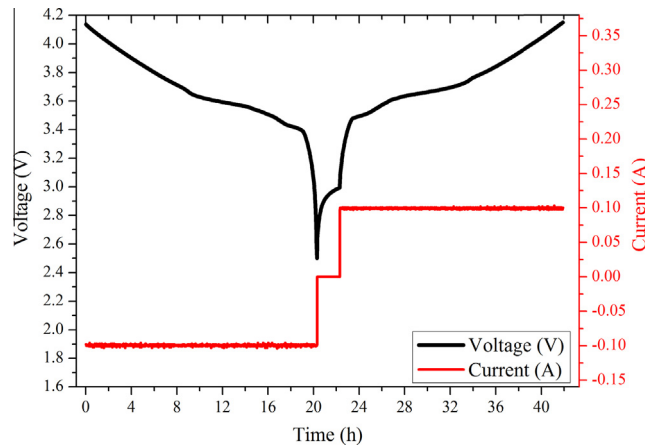


Fig. 2. Current and voltage profile of low-current OCV test.

2.1. OCV-SOC mapping tests

As mentioned above, two OCV test methods were used for OCV-SOC mapping: a low-current OCV-SOC test and an incremental OCV-SOC test. The low-current test used a small current (e.g., C/20, C/25) to charge and discharge the battery so that the corresponding terminal voltage is an approximation of OCV [6,26,29,47]. The incremental OCV test consisted of many SOC intervals and rest periods after which the OCV with the corresponding SOC were observed. Additional data points for the OCV curve were obtained within the SOC intervals using interpolation methods.

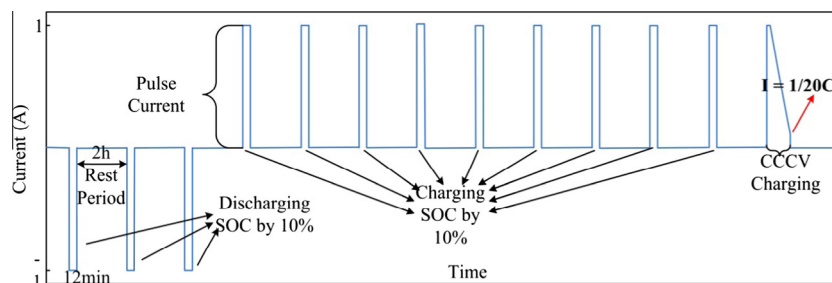


Fig. 3. Test profile of the incremental OCV test.

Fig. 4. Battery test loading profiles: (a) dynamic stress test, (b) Federal Urban Driving Schedule, (c) Highway Driving Schedule, and (d) Beijing Dynamic Stress Test.

2.1.1. Low-current OCV test

In the low-current OCV test, the cell was first charged to its upper cut-off voltage of 4.2 V using a constant current of 1C-rate (1C-rate means that a full discharge of the battery takes approximately 1 h to finish [6]), and then the battery was charged at a constant voltage until its current was reduced to 0.01 C. Secondly, the cell was fully discharged at a constant rate of C/20 until the voltage reached 2.5 V. Then, the cell was fully charged at a constant rate of C/20 to 4.2 V. The terminal voltage at the low C-rate is considered as the equilibrium potential since the small current mini-

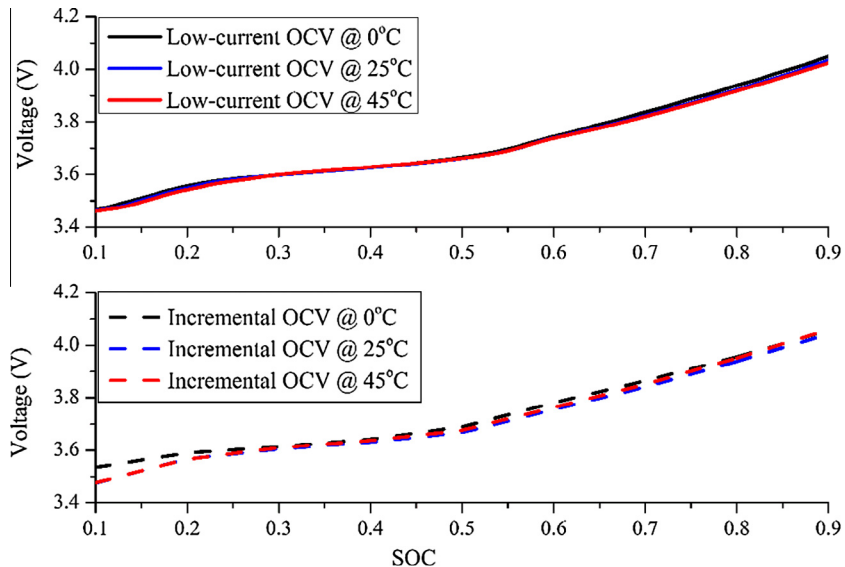


Fig. 5. OCV-SOC curves of two OCV tests at (a) 0 °C, (b) 25 °C, and (c) 45 °C.

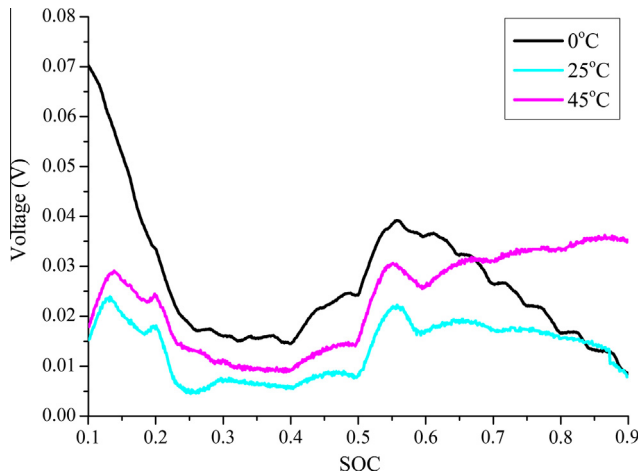


Fig. 6. Difference of measured OCV between two OCV tests at varied temperatures.

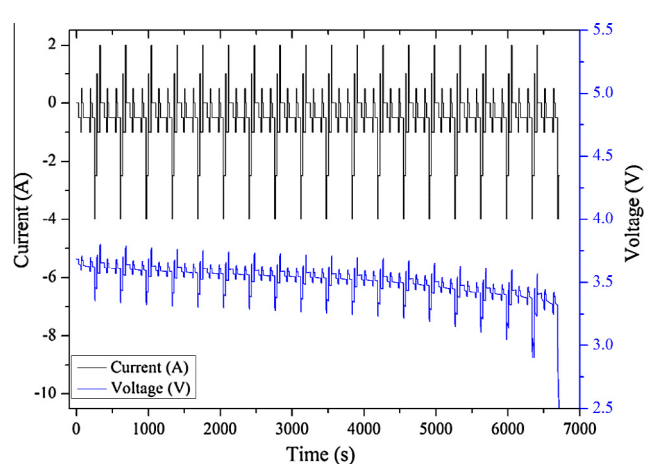


Fig. 8. DST profile at room temperature.

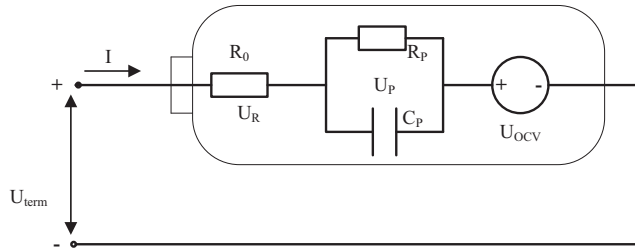


Fig. 7. First-order RC model structure.

mizes the polarization effects inside the cell [26]. Finally, the average voltage of the discharging and charging process was recorded as the OCV, since the effects of hysteresis and ohmic resistance were reduced by the averaging. The corresponding profile of current and voltage using low current is shown in Fig. 2.

2.1.2. Incremental OCV test

In the incremental OCV test, the cell was first fully charged to 100% SOC [39]. Second, the cell was discharged using a negative pulse current-relaxation duration at every 10% SOC. Then, the cell was charged by following the same routine but with a positive

pulse current. Finally, an averaging step and a linear interpolation step were applied to obtain the OCV-SOC curve. The pulse current was set to $C/2$ with a width corresponding to a certain amount of charge (i.e., 10% SOC). At the upper cut-off voltage, a constant voltage (CV) phase was applied until the current became less than $C/20$ to ensure that the cell was fully charged. In addition, the relaxation period was set to 2 to eliminate the polarization effects inside the cell. The current profile of charging with 10 pulse current-relaxation durations is shown in Fig. 3.

2.2. Model parameter identification test

The dynamic stress test (DST) was run on the test samples for model parameter identification. Designed by the US Advanced Battery Consortium (USABC), the DST simulates a dynamic discharge regime and can be scaled down to the desired maximum demand regarding the specified performance of the test samples [48]. The current profile of the DST is shown in Fig. 4(a). Even though the DST consists of a variety of current steps with different amplitudes and lengths and takes into account regenerative charging, it is still a simplification of the real-life loading conditions of batteries [49]. Therefore, in this study the DST was run on the test cells to identify the model parameters.

2.3. Estimators evaluation tests

To evaluate the SOC estimation results (e.g. accuracy, and robustness), several more sophisticated dynamic current profiles

were used: the Federal Urban Driving Schedule (FUDS) [48], the US06 Highway Driving Schedule [50] and the Beijing Dynamic Stress Test (BJDST) [51]. These tests are more complex than the DST in terms of the changing/discharging rate of the current. Sim-

Table 3

Model parameters and statistics list for model comparison.

Temperature (°C)	Estimator using	R_0 (Ω)	R_p (Ω)	C_p (F)	MAE (V)	RMS modeling error
0	Low-current OCV	0.1002	0.0488	1127.6	8.803e-4	0.0021
	Incremental OCV	0.0997	0.0345	619.9	6.895e-4	0.0019
25	Low-current OCV	0.0710	0.0222	1201.4	3.824e-4	6.257e-4
	Incremental OCV	0.0710	0.0342	1135.2	3.708e-4	5.988e-4
45	Low-current OCV	0.0773	0.2133	2469.9	3.910e-4	7.423e-4
	Incremental OCV	0.0770	0.0215	1229.9	3.520e-4	6.041e-4

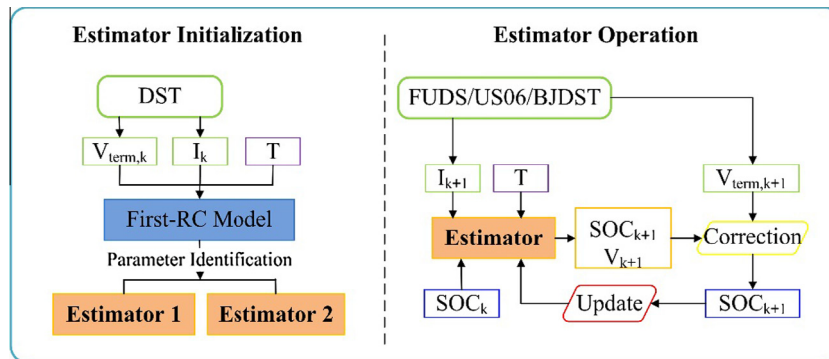


Fig. 9. Block diagram for the SOC estimation procedure.

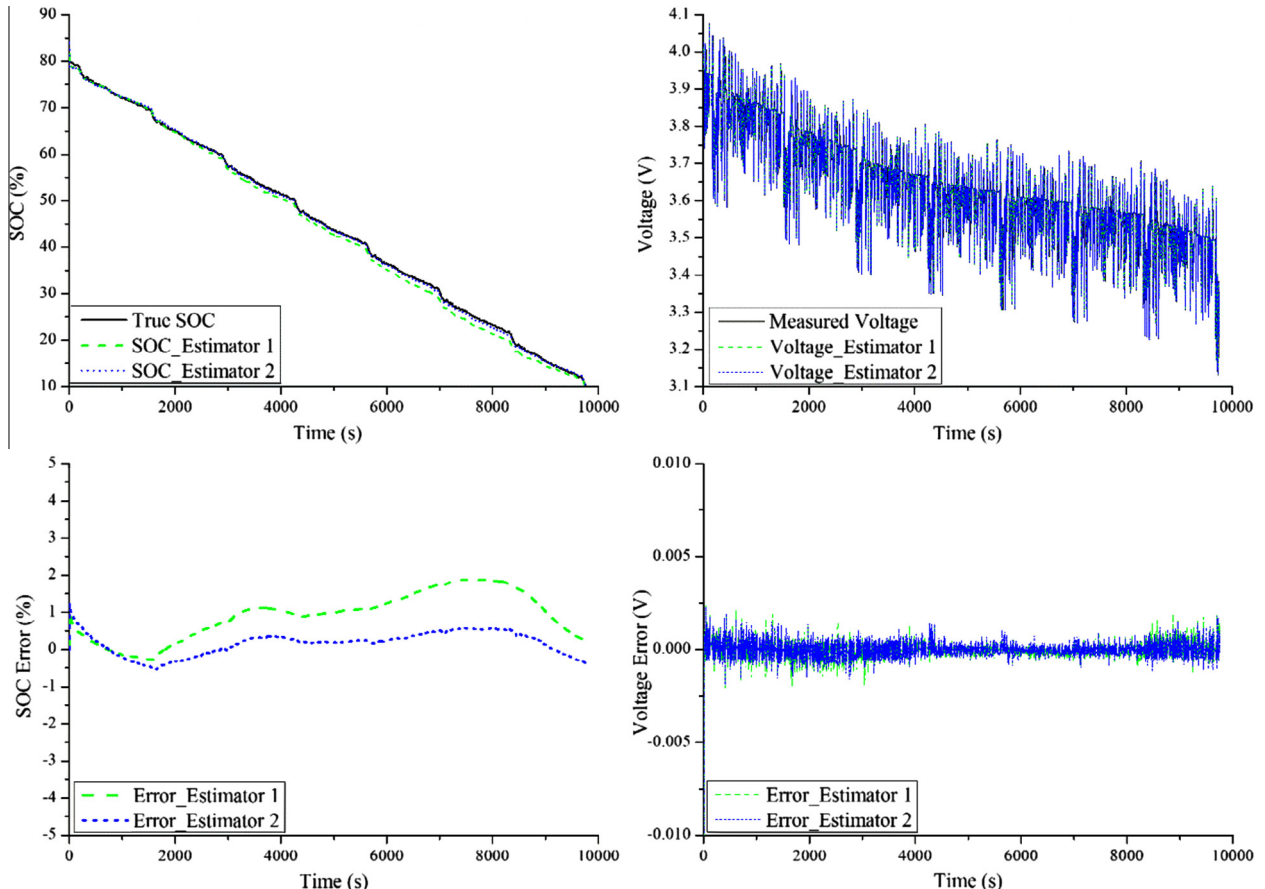


Fig. 10. Results of SOC estimation based on two estimators via FUDS at 25 °C.

ilar to the DST test, the current sequences of FUDS, US06, and BJDST were also transferred from the time-velocity profile of an industry standard automobile. The times for one complete cycle of FUDS, US06, and BJDST are 1372 s, 600 s, and 916 s, respectively. The corresponding current profiles are shown in Fig. 4(b)–(d).

3. OCV-SOC curves of two OCV tests

In the field, lithium-ion batteries used in EVs may face a variety of temperature conditions due to climate and the structural design of the battery pack [52]. Temperature affects the OCV-SOC relationship of lithium-ion batteries. This study investigated the influence of temperature on OCV-SOC curves. In addition, the difference between two OCV-SOC curves was observed to be affected by ambient temperature. Fig. 5 shows the OCV curves of two tests at three ambient temperatures: low, room, and high. The solid line represents the OCV curve obtained by the low-current OCV test, while the dashed line marked in green represents the OCV curve obtained by the incremental OCV test. It can be seen that the low-current OCV curves at three temperatures overlap a lot, especially in the middle range of SOC (i.e., 25–65%). There is a trivial difference among the three curves in the beginning and the end parts of the SOC. Compared with the low-current OCV curves, incremental OCV curves at three temperatures can be distinguished from each other more easily. As shown in Fig. 5(b), the differences between the OCV curve at 0 °C and at 25 °C or 45 °C are quite large (i.e., 0.06 V) when the SOC equals 0.1. Obviously, temperature has an effect on the OCV-SOC relationship, which indicates that tem-

perature should be taken into account when doing SOC estimation. Actually, OCV curves display the electrodes' properties after the relaxation of kinetic processes and provide relevant thermodynamic information [53]. Therefore, OCV curves at different temperatures are supposed to show temperature dependency. From this point of view, an incremental OCV test based-OCV curve describes the battery behavior better since it can reflect voltage difference in terms of ambient temperatures.

Fig. 6 depicts the difference between two OCV test based-OCV curves for varied temperatures. It can be seen that the two OCV curves do not differ much at room temperature. This result makes sense because battery and BMS manufacturers predetermine the OCV-SOC relationship offline using either of the two OCV tests at room temperature, and either of them can lead to an accurate SOC online estimation result. However, the difference between the two OCV curves is relatively large at temperatures other than room temperature. It is interesting to note that the difference at low temperature (0 °C) is greater than that at high temperature (45 °C). The OCV curve difference shows temperature dependency, which implies that the OCV curve difference may become quite large under extreme temperature conditions (i.e., <0 °C). Therefore, there will be significant differences between the SOC estimation results based on two OCV tests at temperatures except room temperature. It makes a lot of sense to investigate the influence of two OCV tests on the SOC estimation results with regard to ambient temperatures. A detailed performance evaluation of the SOC estimator based on two OCV curves is shown in Section 5.

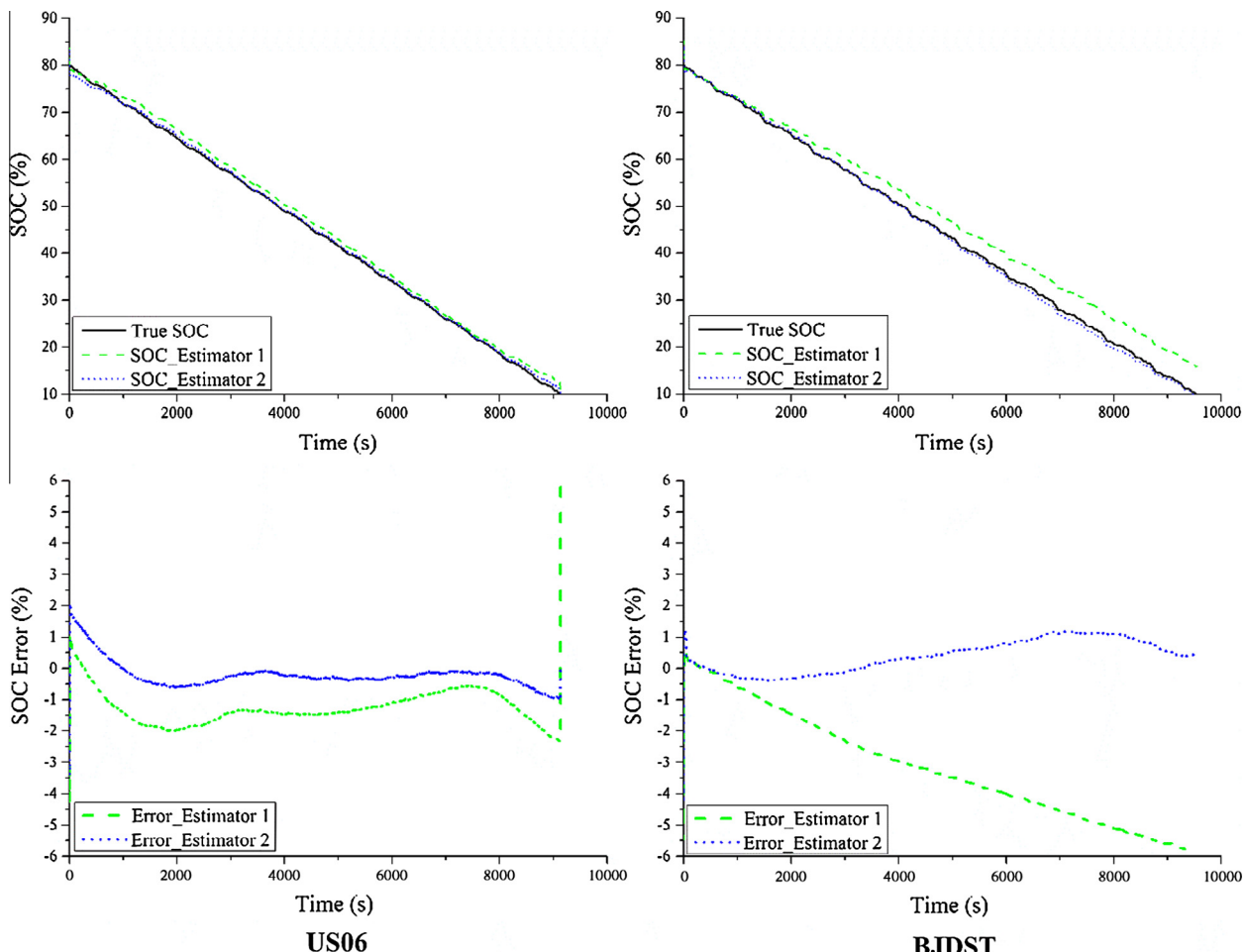


Fig. 11. Results of SOC estimation based on two estimators via US06 and BJDST at 25 °C.

4. Methodology of SOC online estimation

As mentioned in the introduction, an ECM is utilized to model the dynamic behavior of batteries in the BMS for practical applications. Incorporating with battery ECM and an appropriate filtering approach, real-time SOC can be estimated accurately.

4.1. Battery RC model and model identification

For lithium-ion batteries, a first-order RC model that balances estimation accuracy and efficiency shows superiority over other ECMS and thus is employed in this study to model the battery behavior. As shown in Fig. 7, the model consists of three parts: an ideal voltage source U_{oc} , a resistance R_0 , and an RC network that describes the polarization characteristics of a battery. In particular, the transient response during charging and discharging is represented by capacitance, C_p . The dynamic behavior of the battery is shown in Eq. (1).

$$\begin{cases} \dot{U}_P(t) = -\frac{U_P(t)}{R_p C_p} + \frac{I(t)}{C_p} \\ U_{term}(t) = U_{OC}(SOC) + U_P(t) + I(t) \times R_0 \end{cases} \quad (1)$$

where U_{term} is the measured terminal voltage of the battery, U_P is the voltage across the C_p , I is the load current, R_0 is the ohmic resistance, and C_p and R_p are the polarization capacitance and resistance, respectively.

As mentioned in Section 2.2, the DST was run on the test sample to identify model parameters in Eq. (1). To ensure that the sample operated within its design limit, DST was run from 0.8 SOC to low cut-off voltage. The current profile and measured terminal voltage

at room temperature (25 °C) are shown in Fig. 8 with a sampling time of 1 s. The initial SOC is set by the following steps: first, the test sample is fully charged via standard charging based on the sample's datasheet; then the sample is rested for 2 h to eliminate the polarization effects; finally, the sample is discharged at a current rate of 1/2C for 24 min to reach the 0.8 SOC point, which is considered as a true SOC value. Based on the offline OCV-SOC lookup table obtained by two OCV tests, two sets of model parameters (R_0 , R_p , and C_p) were estimated using the least-squares (LS) algorithm. The parameter identification results are shown in Table 3.

Statistical indices, including mean absolute error (MAE) and root mean square (RMS) error, are presented to evaluate the performance of estimators:

$$MAE = \sum_{k=1}^n |f_k - y_k| = \frac{1}{n} \sum_{i=1}^n |e_k| \quad (2)$$

$$RMS \text{ error} = \sqrt{\frac{1}{n} \sum_{k=1}^n (e_k)^2} \quad (3)$$

where f_k is the estimate value, y_k is the true value, and e_k is the modeling error of data set. In this case, battery terminal voltage, $U_{term,k}$, is the value to be compared; thus e_k equals the absolute difference between the estimated $U_{term,k}$ and the measured $U_{term,k}$ at time k . MAE is an index of the average model performance. The smaller the MAE is, the better the model performs. RMS error is the square root of the mean square error, which shows how close a fitted line consisting of estimates is to the measured data points.

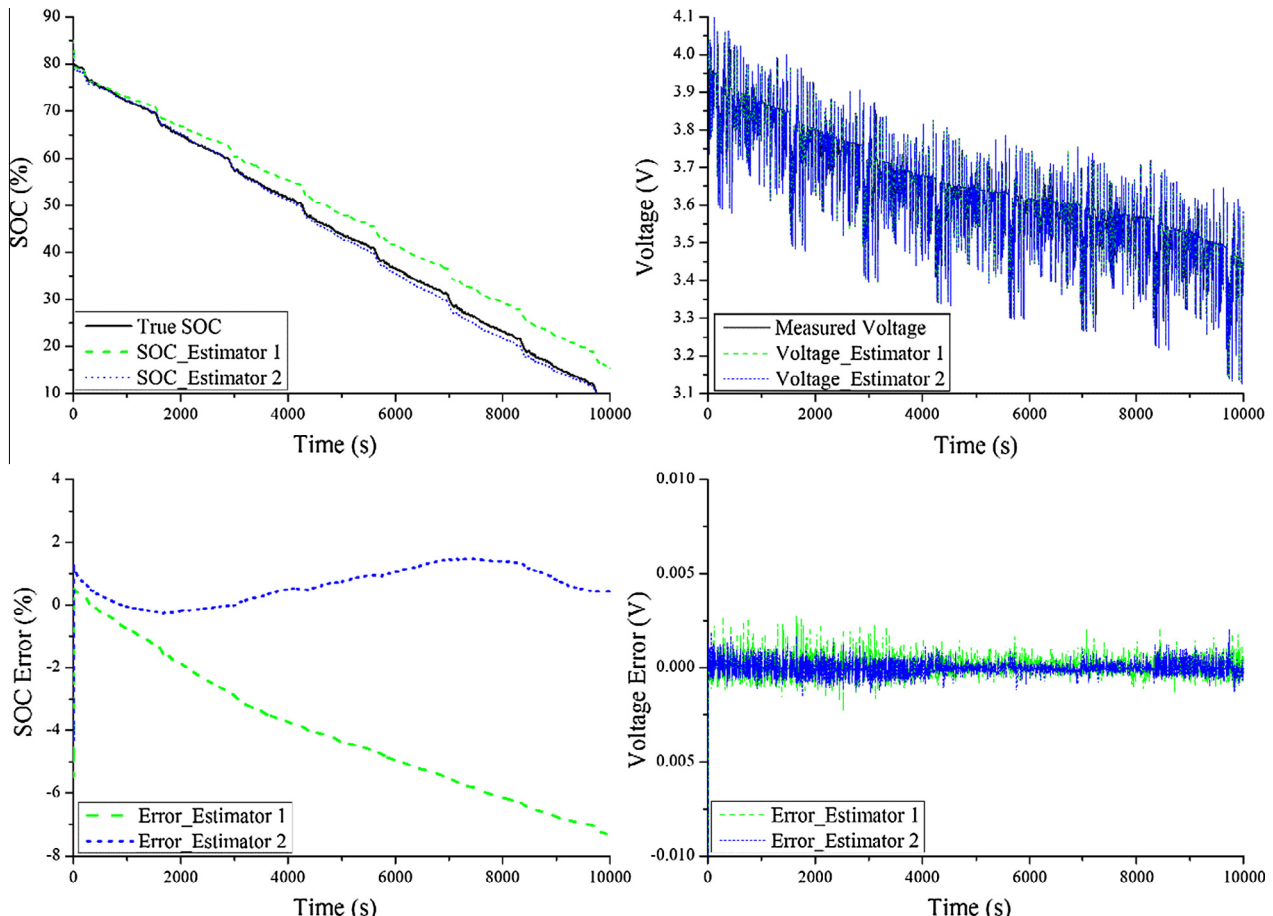


Fig. 12. Results of SOC estimation based on two estimators via FUDS at 45 °C.

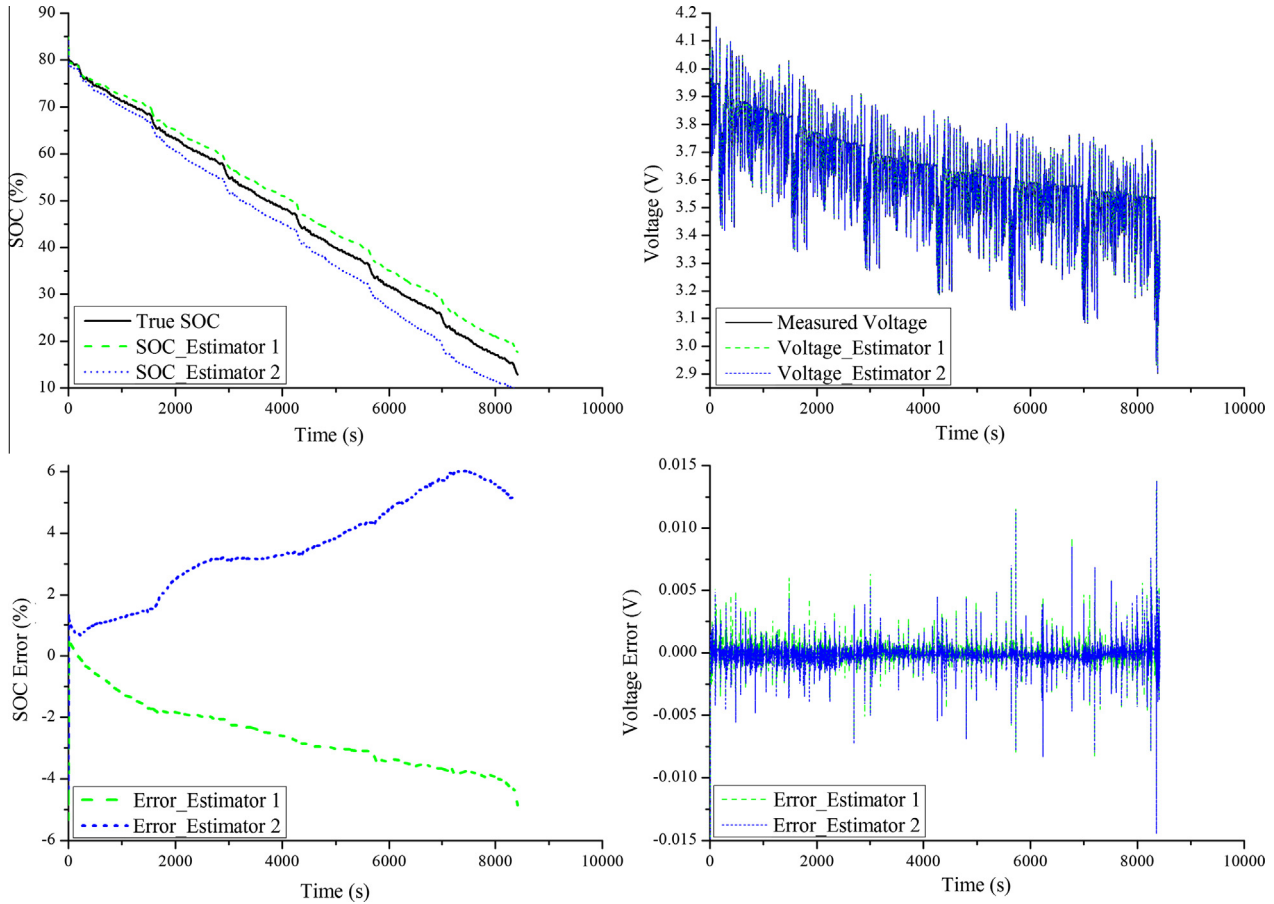


Fig. 13. Results of SOC estimation based on two estimators via FLUDS at 0 °C.

A smaller RMS error value represents a better fit of a model, and 0 is the best. Compared to MAE, the RMS error is more sensitive to large errors and is able to reflect the variation in errors. The SOC estimator using OCV-SOC relationship obtained by low-current OCV test is defined as estimator 1, and the SOC estimator using the OCV-SOC relationship obtained by incremental OCV test is defined as estimator 2. A qualitative assessment of battery modeling results of two estimators is shown via an MAE and RMS modeling error in Table 3. It can be seen that the RMS modeling errors of two estimators are small, and MAEs of two estimators are four orders of magnitude smaller than the voltage working window (2.5–4.2 V) at all three ambient temperatures. In other words, an SOC estimator with either predetermined OCV-SOC relationship can fit the measured data well with regard to temperature. The parameters of each SOC estimator and offline OCV-SOC lookup tables vary with temperature. Thus, a temperature-based SOC estimator for a lithium-ion battery was proposed as follows:

$$\begin{cases} \dot{U}_P(t) = -\frac{U_p(t)}{R_p(T)C_p(T)} + \frac{I(t)}{C_p(T)} \\ U_{term}(t) = U_{OC}(SOC, T) + U_p(t) + I(t) \times R_0(T) \end{cases} \quad (4)$$

4.2. Unscented Kalman filtering for SOC estimation

A battery has an obvious time-varying characteristic, and its online SOC estimation has strong nonlinearity [1]. Compared with the Kalman filter or the extended Kalman filter (EKF), the unscented Kalman filter (UKF) shows strong superiority for reaching the three-order approximation for a nonlinear system. Therefore, UKF was employed for battery SOC online estimation

based on two OCV tests. On the basis of the unscented transform (UT), which describes state distribution by a minimal set of chosen sample points (i.e., sigma points), UKF can represent the mean and covariance of the Gaussian random variables (GRVs) when propagated through a nonlinear system [26]. Thus the state estimation accuracy is improved significantly.

A state space model can be described as follows:

$$\text{State function : } \mathbf{x}_{k+1} = \mathbf{f}(\mathbf{x}_k, \mathbf{u}_k) + \mathbf{w}_k \quad (5)$$

$$\text{Measurement function : } \mathbf{y}_{k+1} = \mathbf{h}(\mathbf{x}_{k+1}, \mathbf{u}_{k+1}) + \mathbf{v}_{k+1} \quad (6)$$

where \mathbf{x}_k is the unmeasurable state vector, which is also a Gaussian random variable; \mathbf{u}_k is the known input vector; \mathbf{y}_k is the measurement vector; $\mathbf{f}()$ is the nonlinear process; $\mathbf{h}()$ is the measurement model; and $\mathbf{w}_k \sim (0, \Sigma \mathbf{w})$ and $\mathbf{v}_k \sim (0, \Sigma \mathbf{v})$ are the zero-mean Gaussian process noise and the zero-mean Gaussian measurement noise, respectively, which reflect the uncertainties due to model inaccuracy and measurement error, respectively.

Incorporating the discrete form of Equation (1) and the coulomb counting principle, a state-space model for SOC estimation via UKF is formulated as follows:

State function:

$$\mathbf{X}_{k+1} = \begin{bmatrix} SOC_{k+1} \\ U_{p,k+1} \\ R_{0,k+1} \end{bmatrix} = \mathbf{A}_k \begin{bmatrix} SOC_k \\ U_{p,k} \\ R_{0,k} \end{bmatrix} + \mathbf{B}_k \mathbf{I}_k + \begin{bmatrix} w_{SOC,k} \\ w_{U_{p,k}} \\ w_{R_{0,k}} \end{bmatrix} \quad (7)$$

Measurement function:

$$\mathbf{Y}_{k+1} = U_{term,k+1} = U_{OC}(SOC_{k+1}) + U_{p,k+1} + I_{k+1} \times R_{0,k+1} + v_{k+1} \quad (8)$$

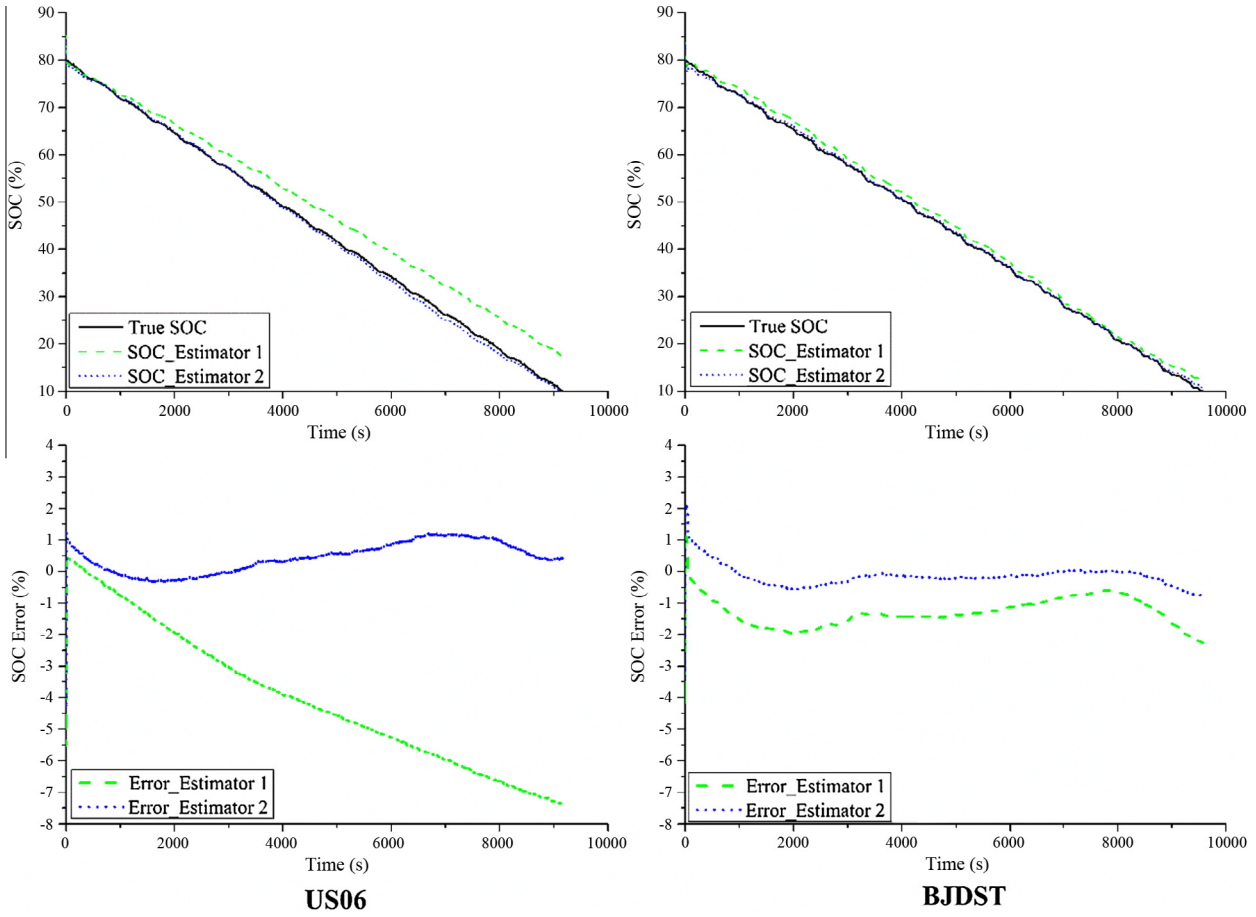


Fig. 14. Results of SOC estimation based on two estimators via US06 and BJDST at 45 °C.

$$\mathbf{A}_k = \begin{bmatrix} 1 & 0 & 0 \\ 0 & \exp(-\Delta t/C_p R_p) & 0 \\ 0 & 0 & 1 \end{bmatrix} \quad (9)$$

$$\mathbf{B}_k = \begin{bmatrix} -\Delta t/C_{real} \\ R_p(1 - \exp(-\Delta t/C_p R_p)) \\ 0 \end{bmatrix} \quad (10)$$

where Δt is the sampling time, which is 1 s in this study, and C_{real} is the maximum available capacity of battery; and $w_{SOC,k}$, $w_{U_p,k}$, $w_{R_0,k}$, and v_{k+1} are zero-mean Gaussian stochastic processes whose covariance are $\sum \mathbf{w}_{SOC}$, $\sum \mathbf{w}_{U_p}$, $\sum \mathbf{w}_{R_0}$, and $\sum \mathbf{v}$, respectively.

5. Results and discussion

In this section, the performance of two SOC online estimators is evaluated and compared from the aspect of both estimator accuracy and robustness. A block diagram is used to illustrate the process of SOC online estimation based on two estimators, as shown in Fig. 9. Notably, the states of both estimators are updated online using the same filtering technique (i.e., the UKF algorithm).

As mentioned previously, ambient temperature is an important factor that influences the ultimate SOC estimation result. Thus, two estimators are compared with regard to varied ambient temperatures. Fig. 10 compares the results of estimated SOC from two estimators at 25 °C in terms of FUDS testing data. The data below 10% SOC is discarded, since the battery is usually operated from 10% to 90% SOC in the field. The black solid line represents the true SOC

value, while the green and blue¹ dashed lines represent the estimated SOCs of estimator 1 and estimator 2, respectively. It can be seen that the black solid line and blue dashed line overlap in Fig. 10(a). In addition, the conclusion can be drawn that estimator 2 gives a more accurately estimated SOC since its error is smaller than the error of estimator 1 during the entire testing time, as shown in Fig. 10(c). The RMSE of SOC estimation for estimator 1 is 1.12%, and that for estimator 2 is only 0.36%. Based on the estimated SOCs, the calculated terminal voltages of two estimators are available and thus can be compared with the real value of the measured terminal voltage of the battery. The comparison results, including terminal voltage and voltage errors, are shown in Fig. 10(b) and (d). The MAE of either estimator 1 or estimator 2 is 0.000291 V, which means that both estimators perform well at estimating battery SOC. However, estimator 1 is relatively better at inferring SOC since it has a smaller RMSE. Therefore, an estimator based on the OCV-SOC relationship from the incremental OCV test can provide a higher accuracy of SOC estimation than an estimator based on the OCV-SOC relationship from the low-current OCV test.

In order to better evaluate the performance of two SOC estimators in a working condition close to a realistic EV operation environment, two more types of high dynamic loading conditions were applied. Fig. 11 compares the results of estimated SOC from two estimators at 25 °C in terms of US06 and BJDST testing data, respectively. In both cases, estimator 2 performed better than esti-

¹ For interpretation of color in Fig. 10, the reader is referred to the web version of this article.

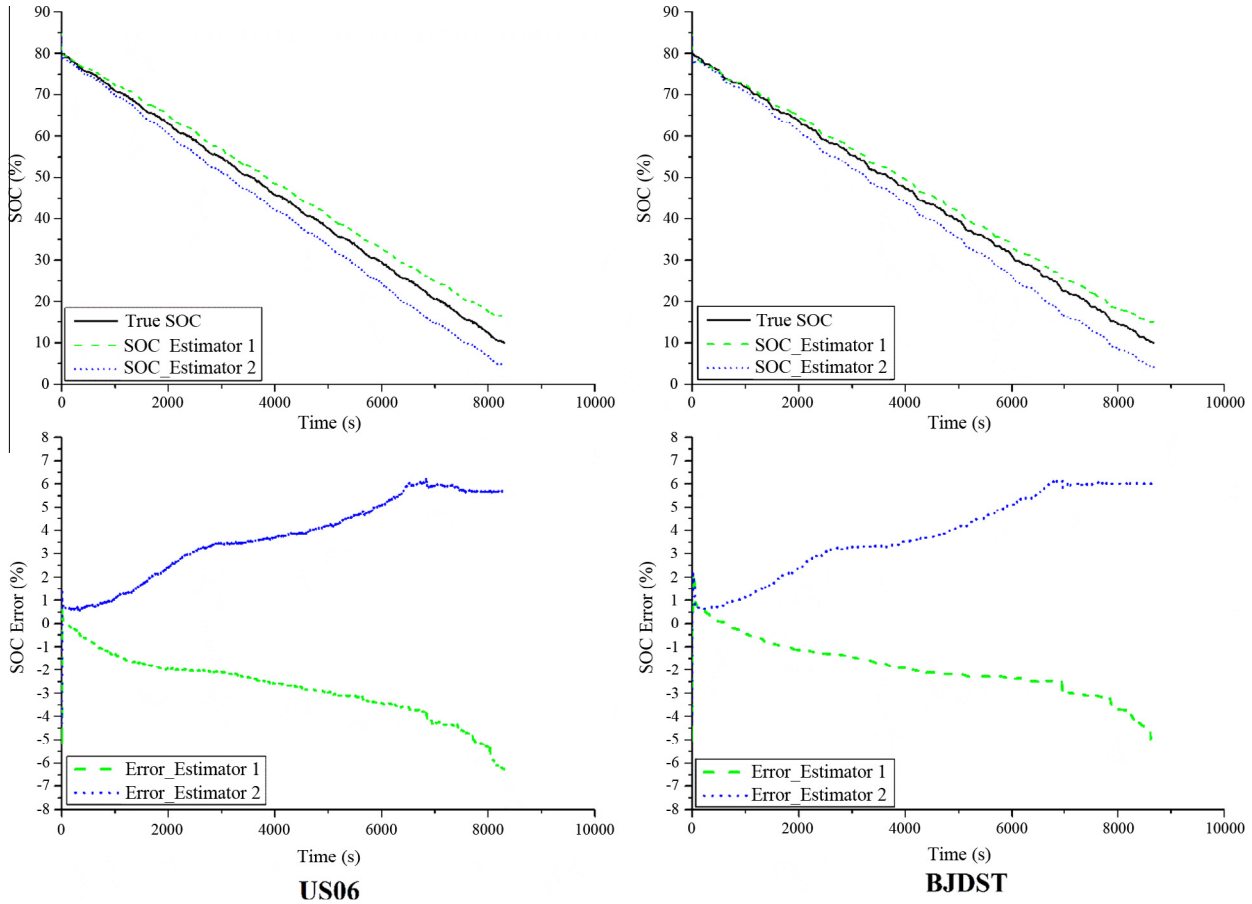


Fig. 15. Results of SOC estimation based on two estimators via US06 and BJDST at 0 °C.

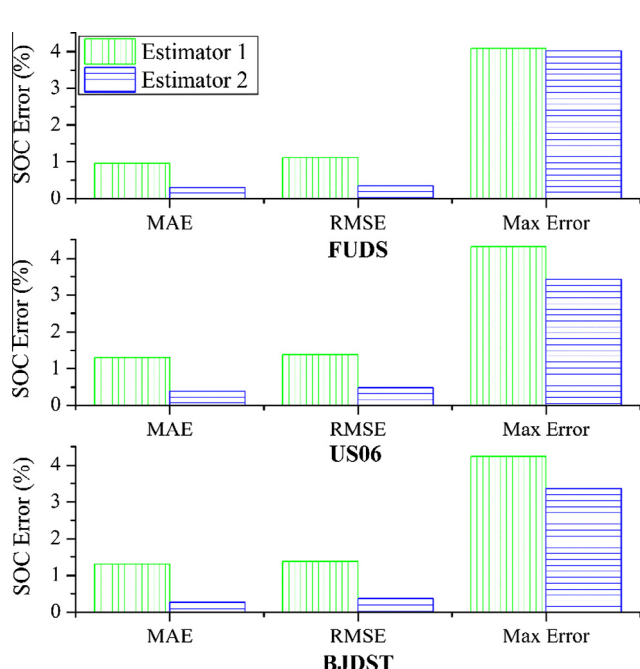


Fig. 16. SOC estimation errors of two estimators at 25 °C under three loading conditions: (a) FUDS, (b) US06, and (c) BJDST.

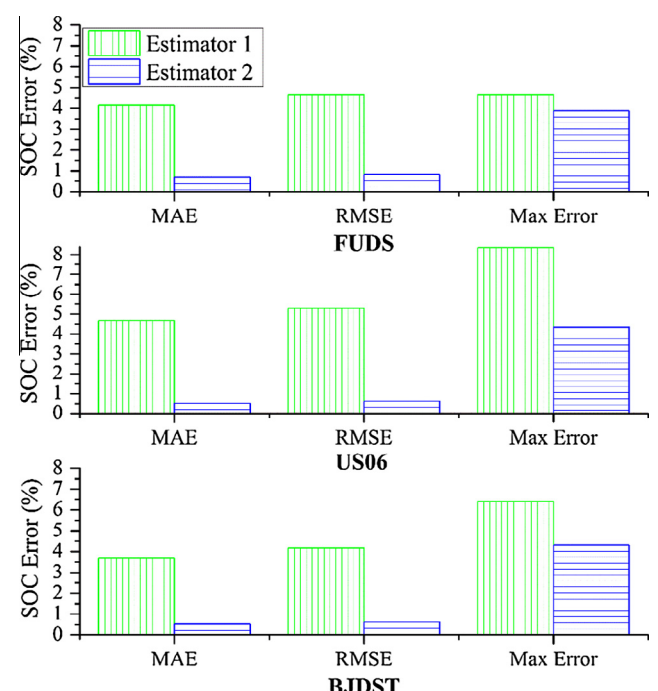


Fig. 17. SOC estimation errors of two estimators at 45 °C under three loading conditions: (a) FUDS, (b) US06, and (c) BJDST.

mator 1 since the blue dashed (SOC of estimator 2) is closer to the black solid line (true SOC). Also, the error of estimator 1 becomes extremely large when the true SOC is around 10% in the condition of US06. The error of estimator 1 becomes larger and larger as the true SOC reduces in the condition of BJDST. Thus, it can be concluded that estimator 2 has higher accuracy than estimator 1 in all loading conditions at 25 °C.

Figs. 12 and 13 show the comparison between estimator 1 and estimator 2 when the FUDS profile was performed at 45 °C and 0 °C, respectively. The RMSE of estimator 1 is 4.65%, and that of estimator 2 is 0.83% at 45 °C, while the RMSE of estimator 1 was 2.78% and that of estimator 2 was 3.90% at 0 °C. The MAE of estimator 1 is 0.000385 V and that of estimator 2 is 0.000292 V at 45 °C, while the MAE of estimator 1 is 0.000502 V and that of estimator 2 is 0.000487 V at 0 °C. Similarly, the performance of two estimators at US06 and BJDST loading conditions are shown in Figs. 14 and 15. The SOC estimation errors of both estimators are becoming larger compared to the errors at room temperature. One reason is that the accuracy of the battery models is less than that at 25 °C, as shown in Table 3. The larger modeling error is possibly caused by the inaccuracy of the OCV-SOC due to the effects of OCV hysteresis. In addition, the two estimators performed more differently at other temperatures than at room temperature. This results from the severer disparity between the low-current OCV test based-OCV curve and the incremental OCV test based-OCV curve at high or low temperatures, as discussed in Section 3. It can be seen that estimator 1 underestimated the battery SOC while estimator 2 overestimated the battery SOC in both the low-temperature and high-temperature cases. Moreover, operation environment uncertainties may cause worse performance of estimators, especially when the battery operates under high dynamic loading conditions [6].

In addition to MAE and RMSE, another evaluation index, the maximum error, was used to compare the two estimators. Fig. 16 shows the SOC estimation errors under different loading conditions at 25 °C. Even though the maximum errors of the two estimators were about the same, the MAE/RMSE of estimator 2 was less than that of estimator 1 under all three loading conditions. The result of the comparison between two estimators at 45 °C is similar. It can be clearly seen that estimator 1 has a higher MAE/RMSE/max error than estimator 2, as shown in Fig. 17. The MAE/RMSE of estimator 2 is one order of magnitude smaller than that of estimator 1, and the maximum error of estimator 2 is at least 1% lower than that of estimator 1. The MAE/RMSE values of estimator 2 under three conditions are around 0.6%, indicating a high accuracy against varying loading profiles. Fig. 18 shows a comparison of two estimators at 0 °C. The maximum errors of two estimators are roughly the same. However, the MAE and RMSE of estimator 1 are lower than that of estimator 2 under three conditions, which is contrary to the comparison results at 25 °C and 45 °C. This is possibly because the low-current OCV test can depict the OCV-SOC relationship better than the incremental OCV test at low temperature. The difference between the two OCV curves (shown in Fig. 6) shows a large deviation when the SOC is low (i.e. 10–30%). Moreover, it can also be seen from Fig. 13(c) that estimator 1 performed better than estimator 2, especially at low SOC ranges.

The true initial SOC was assumed to be knowable in the above-mentioned discussions. However, in reality it is impossible to measure an initial SOC before use due to the measurement error of the voltage sensor and the inaccuracy of the OCV-SOC relationship. Therefore, an error of the guess for the initial SOC is unavoidable. An SOC estimator inside a BMS should have a good self-correction capability. To evaluate the convergence behavior and compare the robustness of the two proposed estimators, this study assumed an initial SOC within ±10% error. Table 4 presents

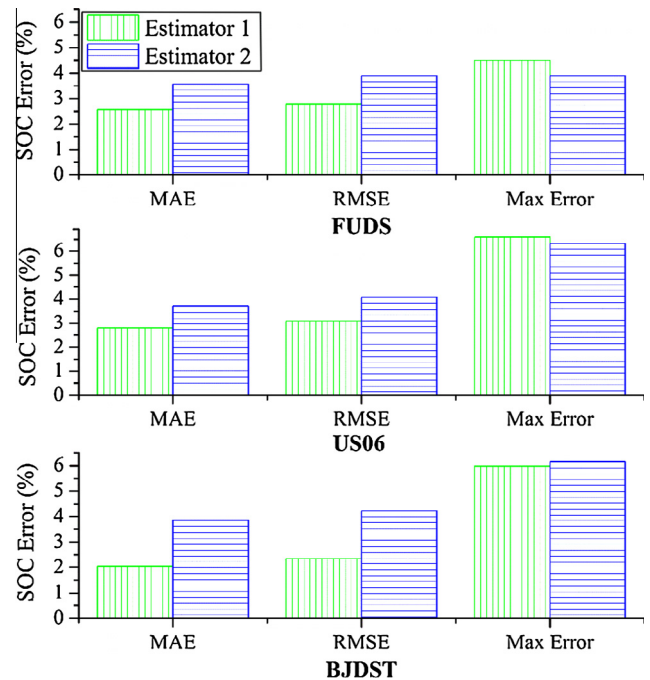


Fig. 18. SOC estimation errors of two estimators at 0 °C under three loading conditions: (a) FUDS, (b) US06, and (c) BJDST.

Table 4
RMSE (%) of two SOC estimators with varied initial guesses.

True initial SOC (%)	Estimator	Error of initial SOC guess		
		0	+10%	-10%
80	Estimator 1	1.1156	1.6979	1.2326
	Estimator 2	0.3585	1.1206	1.2918
50	Estimator 1	2.2602	4.0442	2.7498
	Estimator 2	1.4206	3.7718	2.7135

a comparison of the estimation when the initial guess error of SOC is 0%, +10%, and -10%, while the true initial SOC was 80% under the FUDS loading condition at 25 °C. The RMSEs of the two estimators were calculated and thus the estimation performance was assessed. Overall, the tracking result is satisfactory, as indicated by the RMSEs. Two points should be noted from Table 4. First, estimator 2 showed relatively smaller RMSEs than estimator 1 in all six cases. In particular, estimator 2 showed excellent performance (i.e., the smallest RMSE) when the true initial SOC was 80% and the initial guess was also 80%. Secondly, for each estimator, when the true initial SOC was fixed, a higher initial guess (90%, 60%) led to a smaller RMSE than a lower initial guess (70%, 40%). Fig. 19 shows the comparison results more intuitively. Fig. 16(a) and (c) show a case study where the true initial SOC equals 80%, while Fig. 16(b) and (d) show a case study where the true initial SOC equals 50%. The red solid lines denote the 2% error bound. The estimated error within the error bound means that the SOC estimated result is acceptable in practice. It can be seen that when the true initial SOC is in the high SOC level, both estimated SOCs can converge to the true SOC in 2000 s. In addition, when the initial SOC guess is higher than the true value, estimator 2 performs a shorter period of time in reaching the acceptable estimated SOC. When the initial SOC guess is lower than the true value, the estimated SOC of estimator 1 converged to the true SOC faster than that of estimator 2. However, its performance is less stable than estimator 2, as shown in the huge fluctuation of the error curve at low SOC range (i.e., <20%).

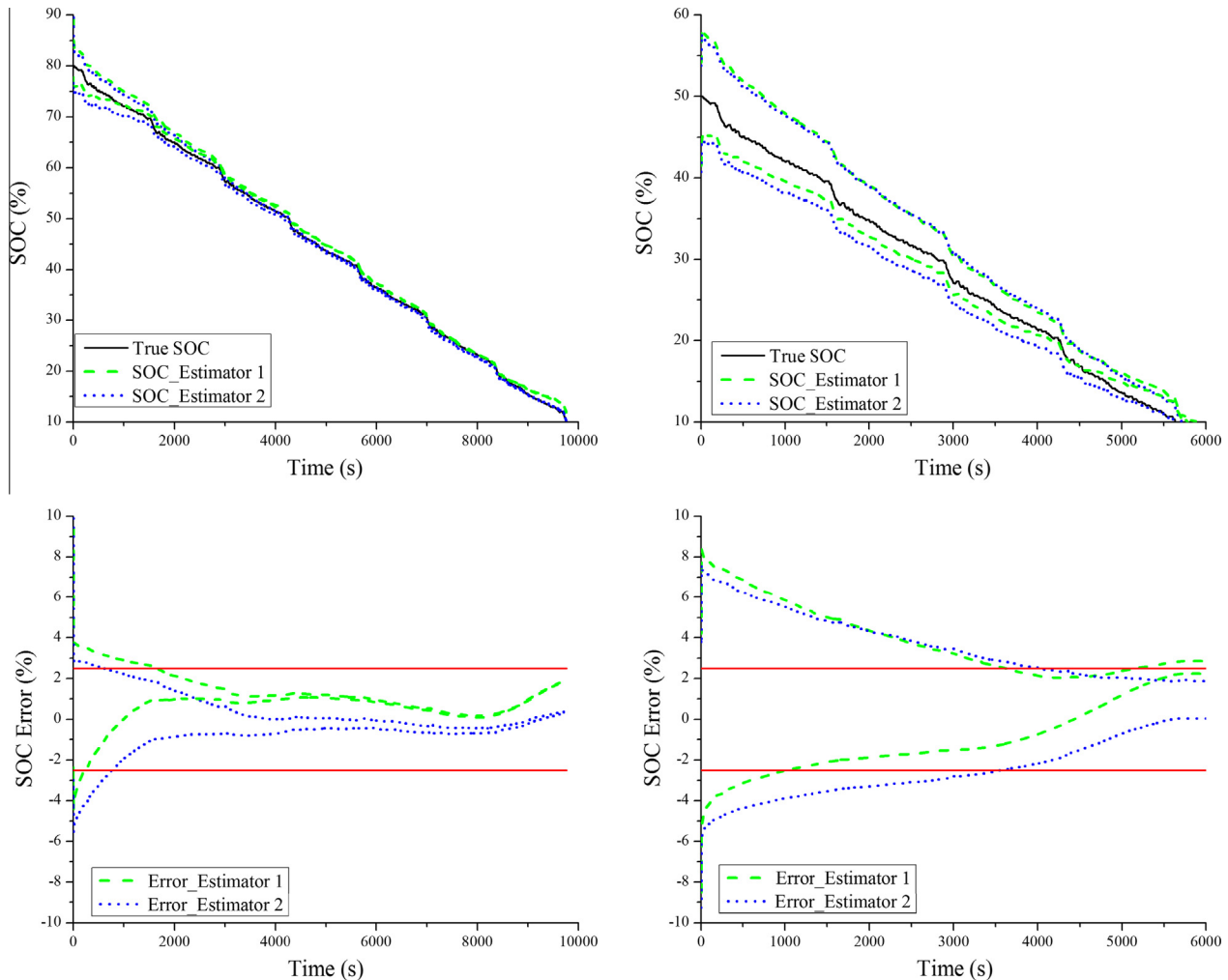


Fig. 19. Comparison between two estimators in convergence behavior at 25 °C.

Based on all the cases discussed above, it can be concluded that estimator 2 has a better overall performance than estimator 1 considering both the accuracy and robustness of SOC estimation. Therefore, this study recommends predetermining offline the OCV-SOC relationship using an incremental OCV test instead of a low-current OCV test. In addition, the temperature effect should be considered in the whole process of establishing an online SOC estimator for practical application in BMSs.

6. Conclusions

As a crucial element of online SOC estimation application for lithium-ion batteries, predetermined OCV-SOC can be observed offline using a low-current OCV test or an incremental OCV test. Both these OCV tests are commonly used by battery manufacturers, BMS designers, and researchers. Based on two OCV tests, two SOC estimators are established. In this paper, two test-based OCV-SOCs were investigated at three temperature conditions. The OCV-SOC relationship is temperature dependent, which means that ambient temperature affects OCV-SOC and, accordingly, influences model-based battery SOC estimation. Moreover, the differences in OCV-SOC values between two tests show temperature dependency (i.e., the difference is smallest at room temperature and higher at other temperatures, especially at low temperature). Therefore, this paper compared the accuracy and robustness of

SOC estimators taking into account ambient temperature. Estimator 2 (based on the incremental OCV test) showed a higher accuracy than estimator 1 (based on the low-current OCV test) at 25 °C and 45 °C. It is notable that estimator 2 did not perform well (i.e., it lost superiority over estimator 1 at 0 °C). A possible reason is that the low-current OCV test provides higher resolution of electrode features than the incremental OCV test at low SOC range. Some detailed OCV-SOC information may be missed due to the linear interpolation processing in an incremental OCV test. Additionally, the robustness against varied loading profiles and against different initial SOC guesses was verified. The results showed that estimator 2 was able to handle loading profile changes and initial guess variations with an RMSE of less than 4%. It can be concluded that the incremental OCV test is more suitable for an approximation of battery OCV-SOC and can provide a more accurate estimated SOC than the low-current OCV test. Thus, this paper recommends employing an OCV-SOC predetermined by the incremental OCV test in lithium-ion BMSs for electric vehicles in real applications.

Due to the lab conditions and limited time, experiments at the temperatures below 0 °C have not been conducted. However, based on our current results at 0 °C, there is a high possibility that performance of two estimators at temperatures below 0 °C will be very different from that at temperatures above 0 °C. Therefore, two OCV tests and the corresponding evaluation will be conducted at

temperatures below 0 °C in our future work. In addition, the temperature dependency of battery OCV-SOC characteristic below 0 °C will also be investigated.

Acknowledgement

This work is supported by the Fundamental Research Funds for the Central Universities (Grant No. 2016YJS144). The authors would like to thank the members of Battery Management and Application Group at the National Active Distribution Network Technology Research Center (NANTEC) at Beijing Jiaotong University and the Battery Group at the Center for Advanced Life Cycle Engineering (CALCE) at the University of Maryland.

References

- [1] He HW, Xiong R, Peng JK. Real-time estimation of battery state-of-charge with unscented Kalman filter and RTOS mu COS-II platform. *Appl Energy* 2016;162:1410–8.
- [2] Lu LG, Han XB, Li JQ, Hua JF, Ouyang MG. A review on the key issues for lithium-ion battery management in electric vehicles. *J Power Sources* 2013;226:272–88.
- [3] Cheng KWE, Divakar BP, Wu HJ, Ding K, Ho FH. Battery-management system (BMS) and SOC development for electrical vehicles. *IEEE Trans Veh Technol* 2011;60:76–88.
- [4] Xing YJ, Ma EWM, Tsui KL, Pecht M. Battery management systems in electric and hybrid vehicles. *Energies* 2011;4:1840–57.
- [5] Scrosati B, Hassoun J, Sun YK. Lithium-ion batteries. A look into the future. *Energy Environ Sci* 2011;4:3287–95.
- [6] Xing YJ, He W, Pecht M, Tsui KL. State of charge estimation of lithium-ion batteries using the open-circuit voltage at various ambient temperatures. *Appl Energy* 2014;113:106–15.
- [7] Piller S, Perrin M, Jossen A. Methods for state-of-charge determination and their applications. *J Power Sources* 2001;96:113–20.
- [8] Aylor JH, Thieme A, Johnson BW. A battery state-of-charge indicator for electric wheelchairs. *IEEE Trans Ind Electron* 1992;39:398–409.
- [9] Liu TH, Chen DF, Fang CG. Design and implementation of a battery charger with a state-of-charge estimator. *Int J Electron* 2000;87:211–26.
- [10] Shen YQ. Adaptive online state-of-charge determination based on neuro-controller and neural network. *Energy Convers Manage* 2010;51:1093–8.
- [11] Salkind AJ, Fennie C, Singh P, Atwater T, Reisner DE. Determination of state-of-charge and state-of-health of batteries by fuzzy logic methodology. *J Power Sources* 1999;80:293–300.
- [12] Shi QS, Zhang CH, Cui NX. Estimation of battery state-of-charge using V-support vector regression algorithm. *Int J Auto Technol* 2008;9:759–64.
- [13] Barsoukov E, Kim JH, Yoon CO, Lee H. Universal battery parameterization to yield a non-linear equivalent circuit valid for battery simulation at arbitrary load. *J Power Sources* 1999;83:61–70.
- [14] Watrin N, Roche R, Ostermann H, Blunier B, Miraoui A. Multiphysical lithium-based battery model for use in state-of-charge determination. *IEEE Trans Veh Technol* 2012;61:3420–9.
- [15] He HW, Xiong R, Fan JX. Evaluation of lithium-ion battery equivalent circuit models for state of charge estimation by an experimental approach. *Energies* 2011;4:582–98.
- [16] Gu WB, Wang CY. Thermal-electrochemical modeling of battery systems. *J Electrochem Soc* 2000;147:2910–22.
- [17] Di Domenico D, Fiengo G, Stefanopoulou A. Lithium-ion battery state of charge estimation with a Kalman Filter based on a electrochemical model. In: *IEEE Int Conf Control Appl*. p. 425–30.
- [18] Di Domenico D, Stefanopoulou A, Fiengo G. Lithium-ion battery state of charge and critical surface charge estimation using an electrochemical model-based extended Kalman filter. *J Dyn Syst Meas Control* 2010;132.
- [19] Marcicki J, Todeschini F, Onori S, Canova M. Nonlinear parameter estimation for capacity fade in lithium-ion cells based on a reduced-order electrochemical model. *P Amer Contr Conf*, 2012.
- [20] Stetzel KD, Aldrich LL, Trimboli MS, Plett GL. Electrochemical state and internal variables estimation using a reduced-order physics-based model of a lithium-ion cell and an extended Kalman filter. *J Power Sources* 2015;278:490–505.
- [21] Corno M, Bhatt N, Savarese SM, Verhaegen M. Electrochemical model-based state of charge estimation for li-ion cells. *IEEE Trans Control Syst Technol* 2015;23:117–27.
- [22] Lee S, Kim J, Lee J, Cho BH. State-of-charge and capacity estimation of lithium-ion battery using a new open-circuit voltage versus state-of-charge. *J Power Sources* 2008;185:1367–73.
- [23] Xiong R, He HW, Sun FC, Liu XL, Liu ZT. Model-based state of charge and peak power capability joint estimation of lithium-ion battery in plug-in hybrid electric vehicles. *J Power Sources* 2013;229:159–69.
- [24] Li XY, Choe SY. State-of-charge (SOC) estimation based on a reduced order electrochemical thermal model and extended Kalman filter. In: *2013 American Control Conference (Acc)*. p. 1100–5.
- [25] Bizeray AM, Zhao S, Duncan SR, Howey DA. Lithium-ion battery thermal-electrochemical model-based state estimation using orthogonal collocation and a modified extended Kalman filter. *J Power Sources* 2015;296:400–12.
- [26] He W, Williard N, Chen CC, Pecht M. State of charge estimation for electric vehicle batteries using unscented kalman filtering. *Microelectron Reliab* 2013;53:840–7.
- [27] Wang JP, Guo JG, Ding L. An adaptive Kalman filtering based state of charge combined estimator for electric vehicle battery pack. *Energy Convers Manage* 2009;50:3182–6.
- [28] Yang FF, Xing YJ, Wang D, Tsui KL. A comparative study of three model-based algorithms for estimating state-of-charge of lithium-ion batteries under a new combined dynamic loading profile. *Appl Energy* 2016;164:387–99.
- [29] Plett GL. Extended Kalman filtering for battery management systems of LiPB-based HEV battery packs – Part 2. Modeling and identification. *J Power Sources* 2004;134:262–76.
- [30] Hu Y, Yurkovich S, Guezennec Y, Yurkovich BJ. Electro-thermal battery model identification for automotive applications. *J Power Sources* 2011;196:449–57.
- [31] Chen M, Rincon-Mora GA. Accurate electrical battery model capable of predicting, runtime and I-V performance. *IEEE Trans Energy Convers* 2006;21:504–11.
- [32] Szumanowski A, Chang YH. Battery management system based on battery nonlinear dynamics modeling. *IEEE Trans Veh Technol* 2008;57:1425–32.
- [33] Hu XS, Li SB, Peng HI, Sun FC. Robustness analysis of State-of-charge estimation methods for two types of Li-ion batteries. *J Power Sources* 2012;217:209–19.
- [34] Weng CH, Sun J, Peng H. A unified open-circuit-voltage model of lithium-ion batteries for state-of-charge estimation and state-of-health monitoring. *J Power Sources* 2014;258:228–37.
- [35] He HW, Xiong R, Guo HQ. Online estimation of model parameters and state-of-charge of LiFePO(4) batteries in electric vehicles. *Appl Energy* 2012;89:413–20.
- [36] Sun FC, Hu XS, Zou Y, Li SG. Adaptive unscented Kalman filtering for state of charge estimation of a lithium-ion battery for electric vehicles. *Energy* 2011;36:3531–40.
- [37] Rahimi-Eichi H, Baronti F, Chow MY. Online adaptive parameter identification and state-of-charge coestimation for lithium-polymer battery cells. *IEEE Trans Ind Electron* 2014;61:2053–61.
- [38] Hu XS, Sun FC, Zou Y. Comparison between two model-based algorithms for Li-ion battery SOC estimation in electric vehicles. *Simul Model Pract Theory* 2013;34:1–11.
- [39] Schwunk S, Armbuster N, Straub S, Kehl J, Vetter M. Particle filter for state of charge and state of health estimation for lithium-iron phosphate batteries. *J Power Sources* 2013;239:705–10.
- [40] Wang YJ, Zhang CB, Chen ZH. Online adaptive parameter identification and state-of-charge coestimation for lithium-polymer battery cells. *Appl Energy* 2014;135:81–7.
- [41] He Y, Liu XT, Zhang CB, Chen ZH. A new model for state-of-charge (SOC) estimation for high-power Li-ion batteries. *Appl Energy* 2013;101:808–14.
- [42] Liu XT, Chen ZH, Zhang CB, Wu J. A novel temperature-compensated model for power Li-ion batteries with dual-particle-filter state of charge estimation. *Appl Energ* 2014;123:263–72.
- [43] Hu XS, Sun FC, Zou Y. Estimation of state of charge of a lithium-ion battery pack for electric vehicles using an adaptive Luenberger observer. *Energies* 2010;3:1586–603.
- [44] Hu XS, Sun FC. Fuzzy clustering based multi-model support vector regression state of charge estimator for lithium-ion battery of electric vehicle. In: *Proceedings of international conference on intelligent human-machine systems and cybernetics, IHMSC'09*. IEEE; 2009. p. 392–6.
- [45] Xiong R, Sun FC, Chen Z, He HW. A data-driven multi-scale extended Kalman filtering based parameter and state estimation approach of lithium-ion polymer battery in electric vehicles. *Appl Energy* 2014;113:463–76.
- [46] Zhang CP, Wang LY, Li X, Chen W, Yin GG, Jiang JC. Robust and adaptive estimation of state of charge for lithium-ion batteries. *IEEE Trans Ind Electron* 2015;62:4948–57.
- [47] Dai HF, Wei XZ, Sun ZC, Wang JY, Gu WJ. Online cell SOC estimation of Li-ion battery packs using a dual time-scale Kalman filtering for EV applications. *Appl Energy* 2012;95:227–37.
- [48] Duong TQ, USABC and PNGV test procedures. *J Power Sources* 2000;89:244–8.
- [49] He W, Williard N, Chen CC, Pecht M. Robust and adaptive estimation of state of charge for lithium-ion batteries. *Int J Electron Power* 2014;62:783–91.
- [50] Maricq MM, Podsiadlik DH, Chase RE. Gasoline vehicle particle size distributions: comparison of steady state, FTP, and US06 measurements. *Environ Sci Technol* 1999;33:2007–15.
- [51] Ma ZY, Jiang JC, Shi W, Zhang WG, Mi CC. Investigation of path dependence in commercial lithium-ion cells for pure electric bus applications: aging mechanism identification. *J Power Sources* 2015;274:29–40.
- [52] Dubarry M, Truchot C, Liaw BY, Gering K, Sazhin S, Jamison D, et al. Evaluation of commercial lithium-ion cells based on composite positive electrode for plug-in hybrid electric vehicle applications III. Effect of thermal excursions without prolonged thermal aging. *J Electrochem Soc* 2013;160:A191–9.
- [53] Petzil M, Danzer MA. Advancements in OCV measurement and analysis for lithium-ion batteries. *IEEE Trans Energy Convers* 2013;28:675–81.